J Mater Sci (2011) 46:1295–1304
DOI 10.1007/s10853-010-4915-4

Compositional dependence of the structural and dielectric properties of Li_2O–GeO_2–ZnO–Bi_2O_3–Fe_2O_3 glasses

Shaaban M. Salem · E. M. Antar · A. G. Mostafa · S. M. Salem · S. A. El-badry

Received: 1 April 2010 / Accepted: 9 September 2010 / Published online: 30 September 2010

Abstract ($10Li_2O$–$20GeO_2$–30ZnO–(40-x)Bi_2O_3–xFe_2O_3 where $x = 0.0$, 3, 6, and 9 mol%) glasses were prepared. A number of studies, viz. density, differential thermal analysis, FT-IR spectra, DC and AC conductivities, and dielectric properties (constant ε', loss tan δ, AC conductivity, σ_{ac}, over a wide range of frequency and temperature) of these glasses were carried out as a function of iron ion concentration. The analysis of the results indicate that, the density and molar volume decrease with an increasing of iron content indicates structural changes of the glass matrix. The glass transition temperature T_g and onset of crystallization temperature T_x increase with the variation of concentration of Fe_2O_3 referred to the growth in the network connectivity in this concentration range, while glass-forming ability parameter ΔT decrease with increase Fe_2O_3 content, indicates an increasing concentration of iron ions that take part in the network-modifying positions. The FT-IR spectra evidenced that the main structural units are BiO_3, BiO_6, ZnO_4, GeO_4, and GeO_6. The structural changes observed by varying the Fe_2O_3 content in these glasses and evidenced by FTIR investigation suggest that the iron ions play a network modifier role in these glasses while Bi_2O_3, GeO_2, and ZnO play the role of network formers. The temperature dependence of DC and AC conductivities at different frequencies was analyzed using Mott's small polaron hopping model and, the high temperature activation energies have been estimated and discussed. The dielectric constant and dielectric loss increased with increase in temperature and Fe_2O_3 content.

S. M. Salem (✉) · A. G. Mostafa · S. M. Salem · S. A. El-badry
Department of Physics, Faculty of Science, Al Azhar University, Nasr City, Cairo 11884, Egypt
e-mail: shaabansalem@gmail.com

E. M. Antar
Department of Radiation Protection and Dosimetry, National Center for Radiation Research & Technology, AEA, Nasr City, Cairo, Egypt

Introduction

Glasses containing bismuth oxide have received increased interest due to their manifold possible applications [1, 2]. These glasses were found to be efficient X-ray absorbers and also considered for use in scintillation detectors for high energy physics [3]. The large polarizability and small field strength of Bi^{3+} in oxide glasses makes them suitable for optical devices such as ultra fast all-optical switches, optical isolators, optical Kerr shutter (OKS) and environmental guidelines. Despite the fact that Bi_2O_3 is not a classical glass former, in the presence of conventional glass formers (such as B_2O_3, PbO, SiO_2, etc.) it may build a glass network of [BiO_n] ($n = 3$, 6) pyramids [4]. In these glasses iron exists in two valence states and electrical conduction occurs by hopping of polaron from Fe^{2+} to Fe^{3+} sites. In the process of hopping, the electron disorders its surrounding, by moving neighboring atoms from their equilibrium positions causing structural defect in the glass network named small polaron. In other words, small polarons are charge carriers trapped by self-induced lattice distortion. Transport of polarons occurs via phonon assisted hopping.

The mobile ionic species in a solid conductor move rapidly through a framework which is formed by other atoms of lattice. This ability of a material to allow movement of ionic species through it can be estimated by detailed study of transport properties like conductivity, diffusion, etc. The ionic conductivity of glasses has been

widely investigated in recent decades [5, 6] and special attention has been devoted to lithium conducting glasses due to their applicability as solid state electrolytes in lithium cells. The factors that are believed to control the magnitude of conductivity in glasses are associated with the composition of the glass network in addition to the binding energies holding the charge carriers in their equilibrium sites and the migration barriers that the carriers face during their transfer [7]. Several models [8, 9] have been advanced to understand the influences of the terms such as type of bonds and charge carriers, polarization in the glass, concentration and mobility of charge carriers to the overall conduction. ZnO is a wide band gap semiconductor and has received increasing research interest. Recent advances have generated more investigations into its application for electronic and optical devices. Furthermore, ZnO can be made a versatile material with broad applications through a proper doping process such as transparent-conducting electrodes (doped with group IIIB, fluorine, and aluminum), piezoelectric as well as ferroelectric layers [10]. The present study is focused on studying the effect of Fe_2O_3 on Li_2O–GeO_2–ZnO–Bi_2O_3 glass system, by means of the density, differential thermal analysis DTA, FT-IR spectroscopy, DC conductivity, and dielectric properties (constant ε', loss tan δ, AC conductivity, σ_{ac}, over a wide range of frequency, and temperature). It is for the first time that the Fe_2O_3 doped Li_2O–GeO_2–ZnO–Bi_2O_3 glasses has been investigated for DC and AC conductivities and dielectric properties over a wide range of frequency and temperature.

Experimental

The ($10Li_2O$–$20GeO_2$–30ZnO–(40-x)Bi_2O_3–xFe_2O_3 where $x = 0.0$, 3, 6, and 9 mol%) glasses, were synthesized by following melt-quenching technique using analytical grade GeO_2, Bi_2O_3, Fe_2O_3, ZnO, and lithium carbonate. The well ground mixture of chemicals in appropriate weight ratios were taken in porcelain crucible and melted in electrical furnace at a constant temperature in the range 1,250 K for an hour. The melt was quickly quenched by pouring on to a stainless steel plate and covering with another stainless steel plate and the random pieces of samples thus formed were collected. Density, d, at room temperature was measured by following Archimedes principle. The carbon tetrachloride, CCl_4 was used as an immersion liquid. The molar volume (V_m), concentration of iron ions, N (cm^{-3}), was calculated using the formula: $N = dPN_A/100A_w$, N_A is Avogadro's number, P the weight percentage of atoms, A_w is the atomic weight, and d is the density. The thermal behavior was investigated using a Shimadzu DTA-50 differential thermal analysis. The temperature and energy calibrations of the instrument were performed using the well-known melting temperatures and melting enthalpies of high purity tin, lead, and indium supplied with the instrument. Samples in the form of powders weighing around 20 mg were sealed in platinum pans in an atmosphere of dry nitrogen at a flow of 30 mL/min and scanned from room temperature to above the exothermic peak at heating rate 10 °C/min. The values of the glass transition temperature, T_g and the peak temperature of crystallization T_p were determined using the software supplied with the apparatus. Infrared spectra of the powdered glass samples were recorded at room temperature in the range 450–1,500 cm^{-1} using a spectrometer (Perkin-Elmer FT-IS, model 1605). These measurements were made on glass powder dispersed in KBr pellets. The DC conductivity measured by means of two-probe method, which appropriate for high resistance materials. Silver painted electrodes were pasted on the polished surface of the samples then situated between two polished and cleaned copper electrodes. The current is monitored by means of a Picometer over temperature range 315–700 K with heating rate 2 K/min, constant voltage source 18.9 V, and a home-made furnace. The AC conductivity (σ_{ac}) has been studied using alternating current measurements, and analyzing their dependence on temperature and frequency. The real dielectric constant ε', AC conductivity (σ_{ac}), and dielectric loss tangent (tan δ) were measured in the temperature range (315–700 K) and over frequency range of (0.12–100 kHz) using a RCL bridge system model [Stanford Res. Model: SR-720].

Results and discussion

Density and DTA

Density determination is an effective method to detect variations in glass structure due to composition or preparing conditions. Some of the most important information that is possible to draw from this measurement is the degree of structural compactness, the modifications of the geometrical configuration of the glassy network, the coordination change of the former ions and the variation of dimensions of the interstitial holes [11]. Thus, Table 1 show that the density decreases 5.43 to 5.16 gm/cm^3 with the increase of Fe_2O_3 concentration in the glass. This indicates that the glass structure becomes less tightly packed with increasing Fe_2O_3 concentration. These trends can be explained rather simply as the replacement of heavier cation Bi by lighter one Fe. Also this result is due to the fact that Fe_2O_3 plays the role of the modifier and introduces excess structural free volume [12].

Differential thermal (DTA) investigations were conducted on the as cast ($10Li_2O$–$20GeO_2$–30ZnO–(40-x)

Table 1 Chemical composition and physical properties of ($10Li_2O$–$20GeO_2$–$30ZnO$–$(40\text{-}x)Bi_2O_3$–xFe_2O_3 where $x = 0.0$, 3, 6, and 9 mol%) glasses

x (mol%)	d (g cm^{-3})	V_m (cm^3/mol)	$N \times 10^{20}$ (cm^{-3})	R (Å)	r_p (Å)	W_{dc} (eV)
0	5.43	43.12	–	–	–	0.99
3	5.31	42.37	4.26	6.16	2.48	0.95
6	5.28	40.79	8.86	4.83	1.94	0.91
9	5.16	40.13	13.5	4.19	1.69	0.88

Bi_2O_3–xFe_2O_3 where $x = 0.0$, 3, 6, and 9 mol%) glasses. The DTA scans exhibit endothermic peaks in the range (498–590 °C) selected as the glass transition temperature, T_g. Crystallization processes taking place in the glass matrix are marked by exothermic peaks T_p in the range (610–655 °C) for all glass samples, the glass transition temperatures, T_g and the onset crystallization temperature, T_x registered for glasses obtained in our glass system shifted to higher temperature with the gradual increase of Fe_2O_3 content. Figure 1 shows the compositional dependence of the glass transition temperatures T_g, the onset crystallization temperature T_x and the difference between T_x and T_g ($\Delta T = T_x - T_g$). With increasing Fe_2O_3 content, the value of T_x and T_g increase, while ΔT decrease, this compositional dependence of T_g can reveal a transformation of the glass structure referred to the growth in the network connectivity. The presence of iron atoms leads to a densification of the Bi_2O_3 glass matrix [13]. The glass-forming ability parameter ΔT, has been frequently used as a rough estimate of the glass formation ability or glass stability. These results apparently indicate that, with the growing presence of Fe_2O_3 in the glass network iron ions mostly increase the cross-link density and enhance the mean bond strength. The decreasing nature of the glass-forming ability parameter ΔT with increasing of Fe_2O_3 indicates an increasing concentration of iron ions that take part in the network-modifying positions.

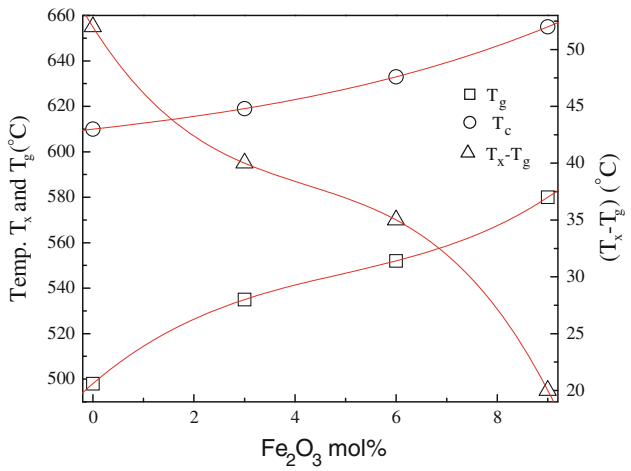

Fig. 1 The composition dependence of the glass transition temperatures T_g, onset crystallization temperature T_x and ($\Delta T = T_x - T_g$)

FTIR spectra

The infrared spectra of glassy samples have been investigated to obtain the information on the structure and arrangement of building structural groups with respect to each other and type of bonds present in the glass. Figure 2 shows the FTIR spectra of ($10Li_2O$–$20GeO_2$–$30ZnO$–$(40\text{-}x)Bi_2O_3$–xFe_2O_3 where $x = 0.0$, 3, 6, and 9 mol%) glasses. The spectra were discussed on the basis of the method given by Tarte [14, 15] and Condrate [16, 17] by comparing the experimental data of glasses with those of related crystalline compounds. In this case the infrared absorption spectra of Fe_2O_3 [16, 18] and α-Bi_2O_3, Bi_2O_3 [18–20] oxides in crystalline phase were used. In FT-IR spectra, the characteristic vibrations of FeO_4 groups in pure Fe_2O_3 and ferrite compounds are ~660 and ~625 cm^{-1}, while for FeO_6 they are at ~580–550 and ~470 cm^{-1} [18, 19]. For α-Bi_2O_3, absorption bands were identified at ~595, 540, 510, 465, 425, and ~380 cm^{-1} characteristic to the vibrations of Bi–O bonds of BiO_6 polyhedra, while in Bi_2O_3 spectra absorption bands were identified at ~840, 620–540, 470, and 350 cm^{-1} characteristic to the vibrations of Bi–O bonds of BiO_3 polyhedra [19]. Due to the fact that the characteristic bands of the investigated glasses were found below 900 cm^{-1}, it was decided to represent the FT-IR spectra only in the region 400–1,200 cm^{-1}. In Fig. 2 the absorption bands were observed for the sample free Fe_2O_3 at ~410, 442, 472, 532, 600, 720, 750, 870, 953, 1020, and 1100 cm^{-1}. The bands observed at ~410, 442, 472, and 532 cm^{-1} which are due to the Bi–O bending vibrations in BiO_6 units [21] and there is a small shoulder near 600 cm^{-1} that was ascribed to the Bi–O$^-$/Bi–O–Zn stretching vibration in the BiO_6 units [22]. The band at ~720 cm^{-1} assigned to Ge–O–Ge stretching vibration in GeO_6 units while the band at ~750 cm^{-1} ascribed to Ge–O bonds vibrations in GeO_4 units [23–26]. At 870 cm^{-1} appears a band due to Bi–O vibration in distorted BiO_6 units [27]. The band at ~953 cm^{-1} can be assigned to Ge–O–Ge stretching vibrations in GeO_4 units while the band at ~1,020 cm^{-1} assigned to the Ge–O stretching vibrations in GeO_4 units [28, 29]. The band at ~1,100 cm^{-1} can be due to the Bi–O–Bi or Bi–O–Ge linkage vibrations [26].

The adding of Fe_2O_3 in the glass matrix produces some change in the FT-IR spectrum, which can be observed by

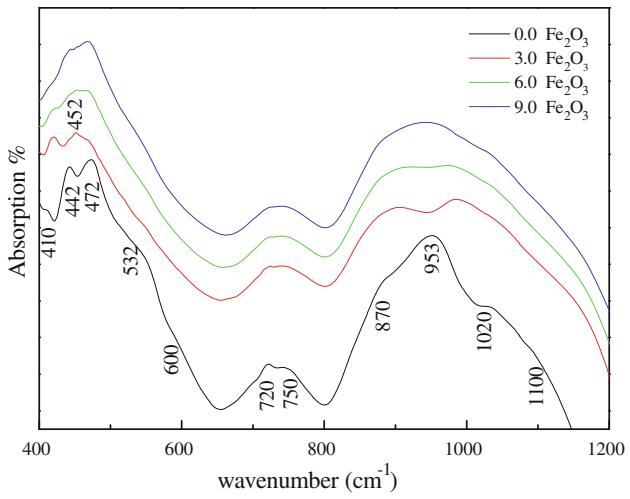

Fig. 2 Infrared absorption spectra of $(10Li_2O–20GeO_2–30ZnO–(40\text{-}x)Bi_2O_3–xFe_2O_3$ where $x = 0.0$, 3, 6, and 9 mol%) glasses

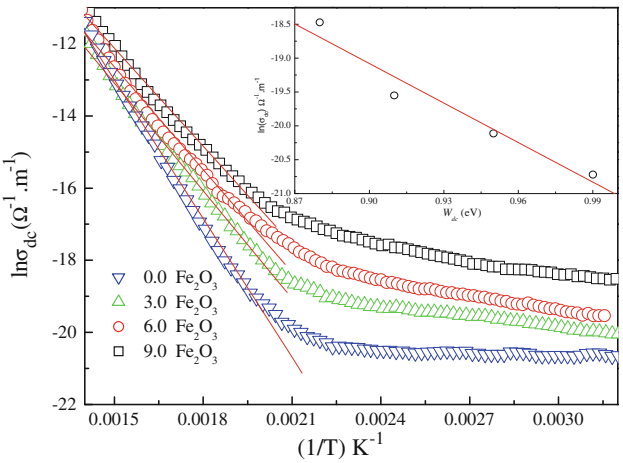

Fig. 3 Temperature dependence of DC conductivity, σ_{dc}, as a function of reciprocal temperature for $(10Li_2O–20GeO_2–30ZnO–(40\text{-}x)Bi_2O_3–xFe_2O_3$ where $x = 0.0$, 3, 6, and 9 mol%) glasses

the appearance of a new band at $\sim$452 cm^{-1} due to the vibrations of Fe–O bonds of FeO_6 units [18, 19]. This band remains unchanged in all compositional range. There is a slight increase in the relative area of the tow bands at $\sim$870 and 1,020 cm^{-1}, which ascribed to stretching vibrations in GeO_4 and BiO_6 units, respectively, with increase iron content in the glass matrix, which can be due to the contribution of the vibrations of Fe–O bonds of FeO_6 units [30–32]. Further increase of Fe_2O_3 content causes increase in the relative area. On the other hand, the relative area of BiO_6 units increases with the increasing of Fe_2O_3 content, while the relative area of GeO_6 units is nearly constant. The increase of these relative areas is probably due to the decrease in the number of non-bridging oxygen atoms once with the increasing of iron ions content. However, the decrease in the number of non-bridging oxygen atoms would increase the connectivity of the glass network. This decrease in the connectivity of the glass network with the increase in Fe_2O_3 content is reflected in the increase of the T_x and T_g. The structural changes observed by varying the Fe_2O_3 content in these glasses and evidenced by FTIR investigation suggest that the iron ions play a network modifier role in these glasses and both Bi_2O_3 and GeO_2 play the role of network formers.

DC conductivity

The temperature dependence of DC conductivity for amorphous semiconductors containing transition metal ions, such as Fe^{2+} and Fe^{3+} for the small polaron hopping conduction, is usually expressed by the Austin–Mott equation [33]:

$$\sigma = (\sigma_o/T)\exp(-W/KT) \quad (1)$$

where, $\sigma_o = (v_o N e^2 R^2/kT)C(1-C)\exp(-2\alpha R)$ is the pre-exponential factor depending on the separation between the conduction carriers, v_o is the Debye frequency for a given solid ($\sim 10^{13}$ Hz), α is the decay parameter of the wave function of the electron in the low valence state ($C = Fe^{2+}/Fe$) is the ratio of concentration of TMI (transition metal ions) in the low valence state to the total concentration of the TMI, R is the average hopping distance $(=1/N)^{1/3}$, W is the activation energy, e is the electronic charge, K is Boltzmann constant and T is absolute temperature. The conductivity data above a typical temperature ($T < \theta_D/2$), where non-linearity is observed in Fig. 3 are fitted with Eq. 1 by least-squares method and the best fit parameters are shown in (Table 2). The small polaron hopping model predicts an appreciable departure from the linear curve of log σ against $1/T$ at a temperature $\theta_D/2$, where θ_D (Debye temperature) is defined by the relation $hv_o = k\theta_D$. Figure 3 shows the variation of logarithm of DC conductivity of $(10Li_2O–20GeO_2–30ZnO–(40\text{-}x)Bi_2O_3–xFe_2O_3$ where $x = 0.0$, 3, 6, and 9 mol%) glasses as a function of inverse temperature T. It is observed that σ increases smoothly with increasing temperature, indicating temperature-dependent activation energy, W, characteristic of small polaron hopping (SPH) conduction mechanism in TMO glasses. Assuming a strong electron phonon interaction, Austin and Mott [33] showed that the activation energy W is the result of polaron formation of binding energy W_p, and an energy difference W_D which might exist between the initial and final sites due to variation in the local arrangements of ions, i.e., $W = W_H + W_D/2$ for $T > (\theta_D/2)$ and $W = W_D$ for $T < (\theta_D/4)$ where W_H is the polaron hopping energy and W_D the disorder energy arising from the energy difference of the neighbors between two hopping sites. The polaron hopping mechanism adiabatic or non-adiabatic can be estimated [34] from a plot of log σ against W at different experimental temperatures T for $(10Li_2O–20GeO_2–30ZnO–(40\text{-}x)Bi_2O_3–xFe_2O_3$ where

Table 2 Physical properties and Polaron hopping parameters of $(10Li_2O–20GeO_2–30ZnO–(40\text{-}x)Bi_2O_3–xFe_2O_3$ where $x = 0.0$, 3, 6, and 9 mol%) glasses

x (mol%)	$v_o \times 10^{13}$ (S^{-1})	W_H (eV)	ε_p	$N(E_F) \times 10^{21}$ ($eV^{-1}m^{-3}$)	γ_p
0	1.98	–	15.81	–	–
3	2.00	0.61	17.76	1.32	29.51
6	2.02	0.63	21.88	2.78	30.57
9	2.04	0.65	24.48	4.41	31.44

$x = 0.0$, 3, 6, and 9 mol%) glasses (inset of Fig. 3). It is expected that the hopping will be in the adiabatic regime if the temperature estimated T_e from the slope of such a plot is close to the experimental temperature, otherwise the hopping will be in the non-adiabatic regime. It is clearly seen that the experimental slope is different from the expected slope $-1/2.303kT$, indicating that the hopping in the present system was non-adiabatic. This non-adiabatic conduction mechanism is further confirmed from the calculation of the polaron bandwidth J,

$$J > (2kTW_H/\pi)^{1/4}(\hbar v_o/\pi)^{1/2} \text{for adiabatic hopping and}$$

$$J < (2kTW_H/\pi)^{1/4}(\hbar v_o/\pi)^{1/2} \text{for non} - \text{adiabatic hopping,}$$

where J is the polaron bandwidth related to the electron wave function overlap on the adjacent sites [35]. The values of $(2kTW_H/\pi)^{1/4}(\hbar v_o/\pi)^{1/2}$ varies from 0.050 to 0.051 eV at 300 K for all the glass concentrations. The values of J independently estimated from the relation [36], $J \approx e^3[N(E_F)/(\varepsilon_o\varepsilon_p)^3]^{1/2}$, varied from 1.19×10^{-3} to 2.88×10^{-3} eV depending on the concentration. J values satisfy $J < (2kTW_H/\pi)^{1/4}(\hbar v_o/\pi)^{1/2}$ which confirms the conduction of the glass of the present system as well as the Fe_2O_3–PbO–Bi_2O_3 glasses [37] to be non-adiabatic SPH. The polaron hopping energy W_H can be calculated from the relation [38] given by

$$W_H = (e^2/4\varepsilon_p)(1/r_p - 1/R) \quad (2)$$

where W_p is the polaron binding energy and $(1/\varepsilon_p) = (1/\varepsilon_\infty) - (1/\varepsilon_o)$, and ε_o and ε_∞ are the static and high-frequency dielectric constant of the glass, respectively, Using W_H, r_p, and R values, we estimated $\varepsilon_p = 15.81$–24.48 (Table 2) which were comparable to those for Fe_2O_3–Bi_2O_3–PbO glasses [37]. We discuss the polaron hopping parameters using the values of R, W_H, and J. The polaron radius r_p for a non-dispersive system of frequency v_o is given by [39].

$$r_p = 1/2(\pi/6N)^{1/3} \quad (3)$$

The density of states at the Fermi level can be estimated as follows [36].

$$N(E_F) = 3/4\pi R^3 W \quad (4)$$

The values of $N(E_F)$ are reasonable for localized states. We estimate the optical phonon frequency, v_o using the experimental data from (Table 1), according to $hv_o = k\theta_D$ h is the Plank's constant. The Debye temperature θ_D was estimated by $T > \theta_D/2$, θ_D of the present glasses was obtained to be 980–952 K. The values of small polaron coupling constant γ_p, which is a measure of the electron–phonon interaction, were also evaluated for the present lasses using the formula $\gamma_p = 2W_H/hv_o$ [40]. The estimated value of γ_p is 29.51–31.44 (Table 2), the value of $\gamma_p > 4$ usually indicates a strong electron phonon interaction [41].

Dielectric constant

The plot of dielectric constant, ε' versus frequency for $(10Li_2O–20GeO_2–30ZnO–(40\text{-}x)Bi_2O_3–xFe_2O_3$ where $x = 0.0$, 3, 6, and 9 mol%) glasses is shown in Fig. 4, at 315 K. It can be noticed that the ε' decreases with increase in frequency and increases with increase in temperature. These measured ε' values of the present glasses are in agreement with the reported ε' values for similar glass system [37]. The dielectric constant of a material is determined by electronic, ionic, dipolar and space charge polarizations. Out of these, the space charge contribution depends on the purity and the perfection of the glass samples. Its influence is in general negligible at very low temperatures and noticeable in the low frequency region. With the gradual increase of the, the values ε', tan δ, and σ are found to increase at any frequency and temperature and activation energy for ac conduction is observed to decrease; this is an indication of an increase in the space charge polarization. Such increase is probably due to the presence of higher concentration of Fe_2O_3 ions in the

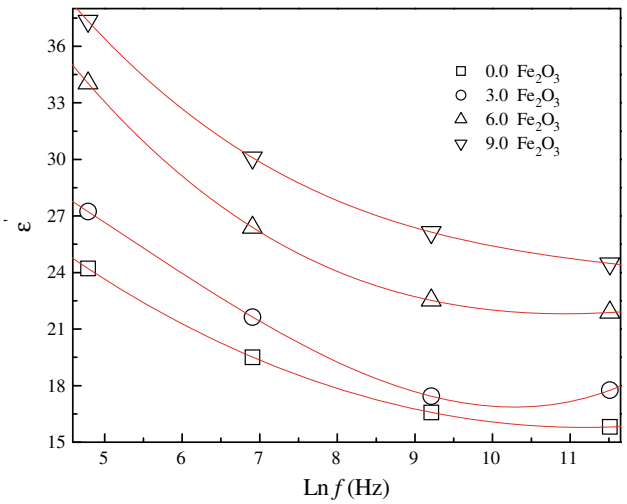

Fig. 4 Plots of ε' versus ln f for $(10Li_2O–20GeO_2–30ZnO–(40\text{-}x)Bi_2O_3–xFe_2O_3$ where $x = 0.0$, 3, 6, and 9 mol%) glasses at 315 K

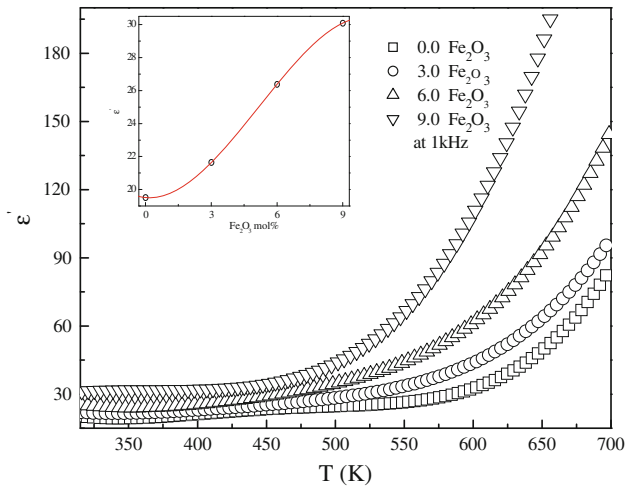

Fig. 5 A comparison plot of variation of dielectric constant with temperature at 1 kHz for ($10Li_2O$–$20GeO_2$–$30ZnO$–$(40\text{-}x)Bi_2O_3$–xFe_2O_3 where $x = 0.0$, 3, 6, and 9 mol%) glasses. *Inset* shows the compositional dependence of dielectric constant, ε' for glass samples at 1 kHz and 315 K

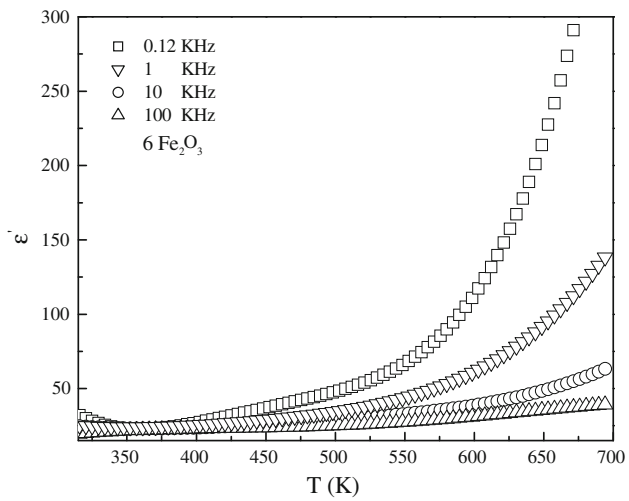

Fig. 6 Variation of dielectric constant with temperature at different frequencies for $x = 6$ mol%

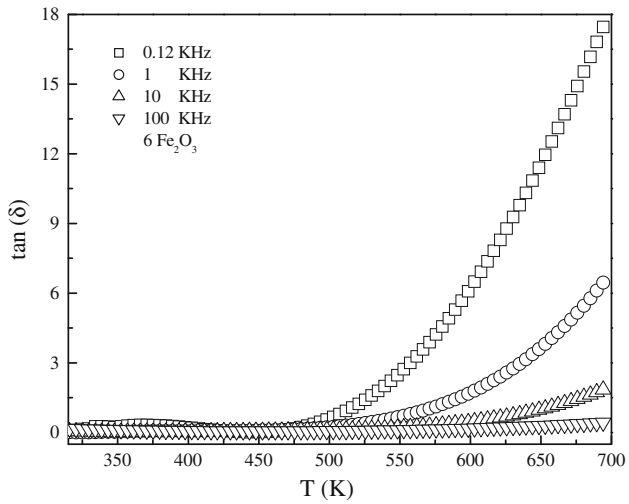

Fig. 7 Variation of dielectric loss with temperature at different frequency for $x = 6$ mol%

glass network that act as modifiers and generate bonding defects in the glass network. The defects thus produced create easy path ways for the migration of charges that would build up space charge polarization and facilitate to an increase in the dielectric parameters as observed [42–44].

The temperature dependence of dielectric constant, ε' of ($10Li_2O$–$20GeO_2$–$30ZnO$–$(40\text{-}x)Bi_2O_3$–xFe_2O_3 where $x = 0.0$, 3, 6, and 9 mol%) glasses is shown in Fig. 5, at 1 kHz. The value of ε' is found to exhibit a considerable increase at higher temperatures. The increase of ε' with increase in temperature is usually associated with the decrease in bond energies [45]. That is, as the temperature increases two effects on the dipolar polarization may occur; (i) it weakens the intermolecular forces and hence enhances the orientational vibration, (ii) it increases the thermal agitation and hence strongly disturbs the orientational vibrations. The dielectric constant becomes larger at lower frequencies and at higher temperatures which is normal in oxide glasses and, is not an indication for spontaneous polarization [46]. This may be due to the fact that as the frequency increases, the polarizability contribution from ionic and orientation sources decreases and finally disappears due to the inertia of the ions. Inset of Fig. 5, shows the variation of dielectric constant with the concentration of Fe_2O_3 measured at 1 kHz. The parameter ε' is observed to increase with the concentration of Fe_2O_3. It is evident that the dielectric constant, ε' increases with increase in Fe_2O_3 concentration. It may be attributed to the increase in electronic contribution to the total polarizability [47]. The compositional dependence of dielectric constant is very much similar to that of AC conductivity. The temperature dependence of dielectric constant, ε' and loss tan δ for the sample containing 6 mol%, are shown in Figs. 6 and 7 at different frequencies, as representing examples of the present glass system. The value of ε' and tan δ is found to increase at higher temperatures especially at lower frequencies. The increase in dielectric constant of the sample with increase in temperature is usually associated with the decrease in bond energies. The dielectric constant becomes larger at lower frequencies and at higher temperatures which is normal in oxide glasses and, is not an indication for spontaneous polarization [48]. This may be due to the fact that as the frequency increases, the polarizability contribution from ionic and orientation sources decreases and finally disappear due to the inertia of the ions. It can be seen that the ε' increases with increase in temperature and at high temperatures it increases more rapidly. This behavior is typical to the polar dielectrics in which the orientation of dipoles is facilitated with rising

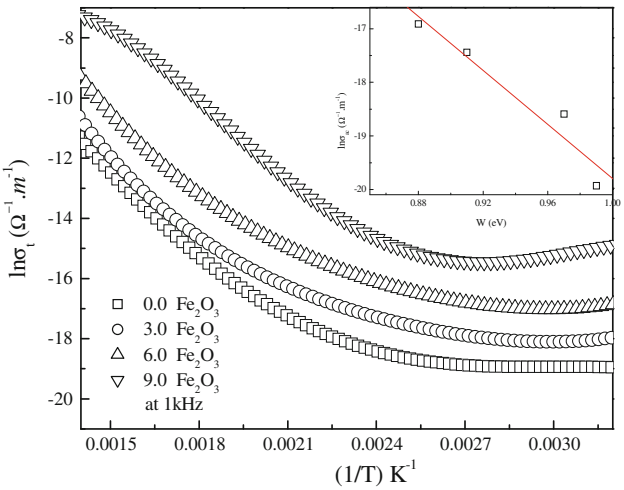

Fig. 8 A comparison plot of variation of ln (σ_t) with $1/T$ measured at 1 kHz for $(10Li_2O–20GeO_2–30ZnO–(40\text{-}x)Bi_2O_3–xFe_2O_3$ where $x = 0.0$, 3, 6, and 9 mol%) glasses. *Inset* shows the plot of log σ_{ac} versus activation energy for conduction

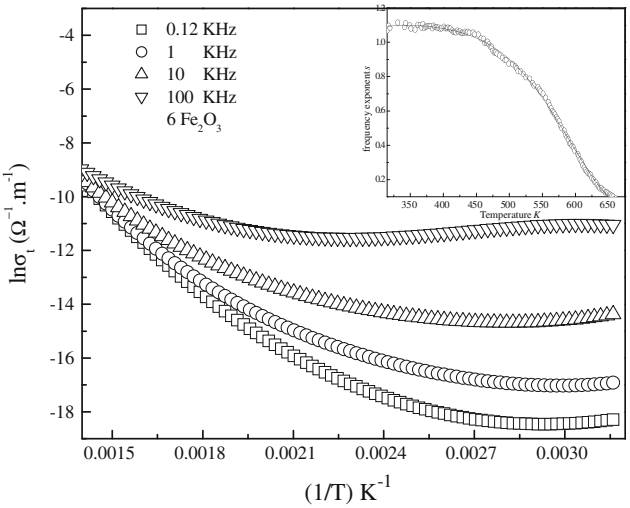

Fig. 9 Plots of ln(σ_t) versus $1/T$ for $x = 6$ mol%, at different frequencies. *Inset* shows the temperature dependence of frequency exponent, *s*. *Solid line* is a fit to CBH model

temperature and there by the dielectric constant is increased. At low temperatures, the contribution of electronic and ionic components to the total polarizability will be small. As the temperature is increased the electronic and ionic polarizability sources start to increase [49].

AC conductivity

The temperature dependence of $\sigma(\omega)$ conductivity in $(10Li_2O–20GeO_2–30ZnO–(40\text{-}x)Bi_2O_3–xFe_2O_3$ where $x =$ 0.0, 3, 6, and 9 mol%) glasses has been depicted in Fig. 8, at 1 kHz. Inset of this figure shows a plot of log σ against W at 315 K. The value of AC conductivity σ is found to increase at higher temperatures especially at lower frequencies. From these plots, the activation energy for conduction in the high temperature region over which a near linear dependence of log σ_{ac} with $1/T$ calculated and presented in Fig. 9, and (Table 3). When a plot is made between log $\sigma(\omega)$ versus activation energy for conduction (in the high temperature region) a near linear relationship is observed (inset of Fig. 8); further, the variations of the conductivity (at 315 K) and the activation energy for conduction, with the concentration of Fe_2O_3 show an opposite trend (Fig. 10). These observations suggest that the conductivity enhancement is directly related to the thermally stimulated mobility of the charge carriers in the high temperature region. The temperature dependence of AC conductivity $\sigma(\omega)$ for $x = 6$ mol%, has been depicted in Fig. 9, at different frequencies. Inset of this figure shows the temperature dependence of frequency exponent, *s*. Solid line is a fit to CBH model. The values of ε', tan δ and also AC conductivity are found to increase at any frequency and temperature with increase in the concentrations of Fe_2O_3. In the studied

Table 3 Electrical parameters of $(10Li_2O–20GeO_2–30ZnO–(40\text{-}x)Bi_2O_3–xFe_2O_3$ where $x = 0.0$, 3, 6, and 9 mol%) glasses

x (mol%)	W_{ac} (eV)	W_M (eV)	R_ω/R	R_ω (Å)	S	$\ln\sigma_o$ $(\Omega m)^{-1}$
0	0.99	–	–	–	0.82	2.86
3	0.97	0.986	0.343	2.11	0.98	2.53
6	0.91	0.927	0.345	1.67	1.11	2.22
9	0.88	0.897	0.347	1.45	0.85	1.98

glasses iron ions (both Fe^{2+} and Fe^{3+}) occupy octahedral positions, act as modifiers and create bonding defects. The defects thus produced create easy path ways for the migration of charges that would build up space charge polarization leading to an increase in the dielectric parameters. The frequency dependent conductivity $\sigma_{ac}(\omega)$ increases approximately linearly with angular frequency ω:

$$\sigma_{ac} = \sigma_t - \sigma_{dc} = A\omega^{S(T)} \quad (5)$$

where $s(T)$ the frequency exponent, σ_{dc} is the DC conductivity and $\sigma_{ac} = A\omega^{s(T)}$ and σ_t is the total conductivity, which is actually the measured factor in an AC, experiment. The low frequency region is dominated by the DC conductivity while the high frequency part presents power law behavior. The frequency exponent s values were calculated calculated at a high frequency limit from the slopes of ln σ_{ac} vs. ln F plots. Figure 11 shows log σ_{ac} versus log F plots obtained for the sample containing 6 mol%. From Fig. 11, it is observed that the frequency dependent of conductivity shows two distinct regimes, within the measured frequency window, (i) the low frequency plateau region and (ii) high frequency dispersion region. The plateau region corresponds to frequency independent conductivity σ_{dc}. For the present glasses, the

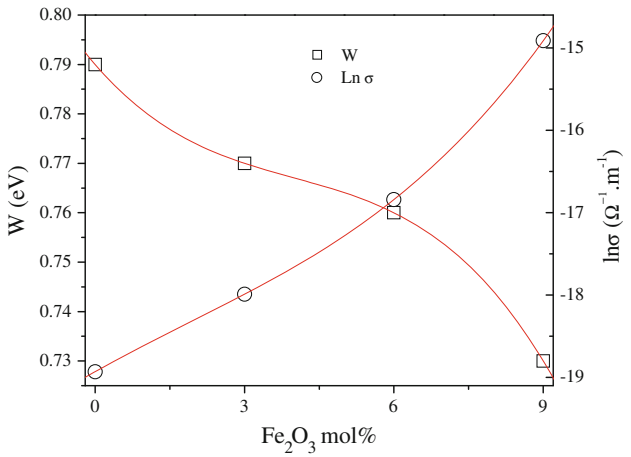

Fig. 10 The variation of log $\sigma(\omega)$ and the activation energy for conduction as function of Fe_2O_3 content

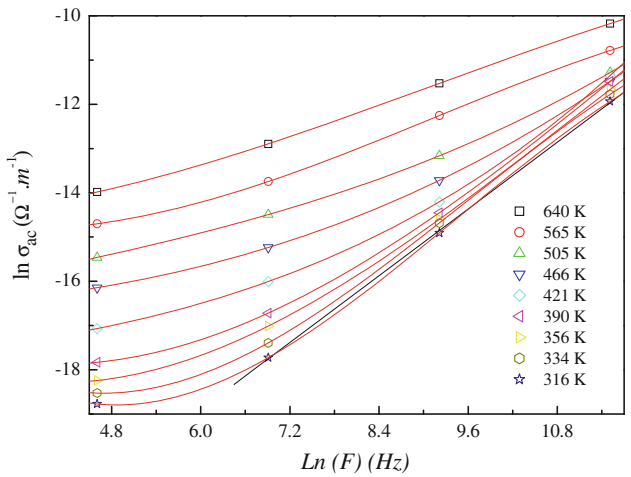

Fig. 11 The plot of AC conductivity, ln (σ_{ac}), versus ln (F) for sample containing $x = 6$ mol%. *Solid lines* are the best fits to Eq. 5

frequency exponent, s, values were determined at a high frequency limit to belying between 1.11 and 0.82 in the studied system. (Table 3), indicates no systematic variation of s with composition. However, the decreasing trend of s with temperature can be noticed. This kind of variation of s with temperature has been observed in different TMI/alkali doped borate [50] and phosphate [51] glasses. The observed variation of s with temperature may be due to different contributions from conducting and dielectric losses at different temperatures [50, 51]. There are theoretical models [45, 52–54] which predict the temperature dependence of frequency exponent, s, such as simple quantum mechanical tunneling QMT, temperature-dependent QMT and correlated barrier hopping (CBH) models. The distinction between lattice and carrier responses is that they correspond to intrinsic and extrinsic processes, respectively, due to some impurities or injected carriers as a result of the existence of transition metal ions. According to Elliott [55] the correlated barrier hopping (CBH) model was proposed and was applied to the chalcogenide glassy semiconductors as well as to oxide glasses [55]. In this model the bipolaron has been proposed to interpret the frequency dependent conductivity. This model was successful in explaining many temperature-dependent conductivity results at low temperature. However, it does not explain the high temperature behavior particularly in the low frequency range. This theory was extended to high temperature by assuming a single polaron hopping [56], where it produces more satisfactory results. In this respect ac conductivity given for correlated narrow-band limit for random sites and single polaron hopping [53] as:

$$\sigma_{ac}(\omega) = (1/24)\pi^3 \varepsilon_o \varepsilon' \omega (R_\omega/R)^6 \quad (6)$$

the hopping distance R_ω at frequency ω is given by;

$$R_\omega = e^2/\pi\varepsilon_o\varepsilon'[W_M - KT\ln(1/\omega\tau_o)] \quad (7)$$

where e is the electronic charge, ε' is the dielectric constant, ε_o is the dielectric constant of free space, W_M the maximum barrier height, τ_o is the Debye relaxation time is of the order 10^{-13} s [41], and K is the Boltzmann constant. On applying Eq. 6 to the experimental AC conductivity data it was found that the factor (R_ω/R) is in the range (0.343–0.347 Å) as a function of composition and frequency for the present system, see (Table 3), These results indicate a hopping distance R_ω (1.45–2.11 Å), up to 315 K, using the permittivity data when the exponent s, is active, i.e., for frequencies above 1 kHz,. (Table 3) collects the obtained results. On the contrary, the frequency dependent conductivity in the CBH model can be expressed in terms of the frequency exponent s, as:

$$S = 1 - 6KT/[W_M - KT\ln(1/\omega\tau_o)] \quad (8)$$

In the CBH model electrons in charged defect states would hop over the coulombic barrier of height W, given as; $W = W_M - [ye^2/\pi\varepsilon_o\varepsilon R]$, where y is the number of electrons to hop ($y = 1$ for single polaron case and $y = 2$ for the bipolaron case), and e the electronic charge. As shown inset of Fig. 9, it is noted that s decrease with temperature. This suggests that the correlated barrier hopping conductivity (CBH) is dominant in ac conductivity mechanism of the present glass system.

The composition dependence of log σ_{ac} and activation energy W_{ac} is shown inset of Fig. 10. The activation energy is found to decrease while the AC conductivity increases with increase in Fe_2O_3 content this result is accord with that obtained from DC conductivity as shown in (Fig. 12). Since the AC conductivity is associated with the migration of polaron between Fe^{2+} and Fe^{3+} ions with the distribution in hopping distance it seems that increase in Fe_2O_3 content decreases the distance between Fe ions. Such

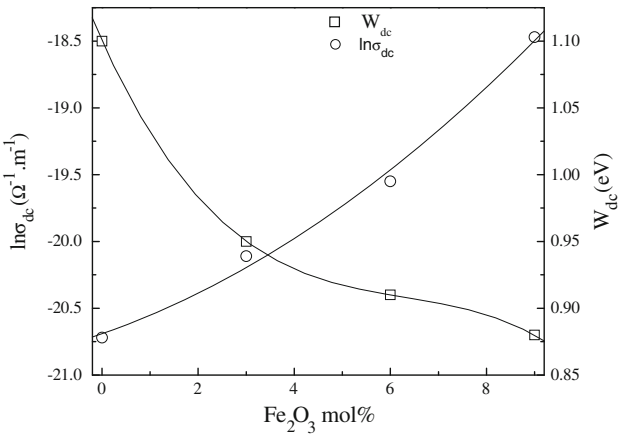

Fig. 12 Effect of Fe_2O_3 content on dc conductivity, σ, and activation energy, *W*. *Lines* are drawn as guides for the eye

decrease in the distance between Fe ions enhances the probability of electron hopping and increases the ac conductivity and decreases the activation energy for conduction [57]. On the other hand, increase of conductivity with the increase of Fe_2O_3 content in the glass system is a manifestation of increasing concentration of mobile electrons, or polarons, involved. Based on quantum mechanical tunneling model, $N(E_F)$ is the density of the energy states near the Fermi level have been evaluated from dc conductivity data and values obtained are presented in (Table 2). The value of $N(E_F)$ obtained $\approx 10^{21}$ eV^{-1} cm^{-3}, such values of $N(E_F)$ suggest the localized states near the Fermi level are responsible for conduction. Further, the value of $N(E_F)$ is found to increase gradually with the increase of Fe_2O_3 content, indicating an increase in the degree of disorder in the glass network. When a plot is made between log σ_{ac} versus activation energy for conduction, a near linear relationship is observed inset of Fig. 8, the near linearity between the conductivity and the activation energy suggests the conductivity enhancement is directly related to the increasing mobility of the charge carriers. Since the Li^+ ions are more mobile than all the other ions (like Fe ions) can be regarded as virtually immobile with in the time window of hopping processes of the alkali (Li^+) ions [58]. Therefore, the contribution to the conduction for the present glasses in the high temperature region can be mainly considered due to monovalent lithium ions.

Conclusions

Glasses of ($10Li_2O$–$20GeO_2$–$30ZnO$–$(40\text{-}x)Bi_2O_3$–xFe_2O_3 where $x = 0.0$, 3, 6, and 9 mol%) glasses, were prepared and investigated by Differential thermal analysis DTA, density, FT-IR spectroscopy in order to obtain information about their structure and to point out the role of each component of the glass system in the forming of the glass network, dielectric constant ε', loss tan δ and AC conductivity σ_{ac} over a moderately wide range of frequency and temperature, and frequency exponent *s*. The density and the molar volume are decreasing monotonous with the increasing of the iron content in all compositional range. The DTA results evidenced that, the value of the glass transition temperature T_g and glass-forming ability parameter ΔT have been observed to decrease with increase in the concentration of Fe_2O_3. These results apparently indicate that, with the growing presence of Fe_2O_3 in the glass network iron ions mostly occupy network-forming positions, increase the cross-link density and enhance the mean bond strength. The decreasing nature of the glass-forming ability parameter ΔT with increasing of Fe_2O_3 indicates an increasing concentration of iron ions that take part in the network-modifying positions. The FT-IR spectra evidenced that the main structural units are BiO_3, BiO_6, ZnO_4, GeO_4, and GeO_6. On the other hand FeO_6 structural units can be observed but the presence of FeO_4 structural units cannot be excluded. The temperature dependence of AC and DC conductivity at high temperatures has been explained using Mott's small polaron hopping model. The AC and DC conductivity increased and activation energies decreased with increase of Fe_2O_3 content at all frequencies. Based on these results it is concluded that iron ions, enhances the electronic motion. The frequency dependent conductivity has been explained by correlated barrier hopping model as the frequency exponent, *s* values due to CBH model agreed with the experimental values of *s*. Both ε' and tan δ increased with increase in temperature and Fe_2O_3 concentration.

References

1. Bale S, Srinivasa Rao N, Rahman S (2008) Solid State Sci 10:326
2. Bale S, Purnima M, Srinivasu CH, Rahman S (2008) J Alloys Compd 457:545
3. Bishay A, Maghrabi C (1969) Phys Chem Glasses 10(1):1
4. Dumbaugh WH (1986) Phys Chem Glasses 27:119
5. Ingram MD (1987) Phys Chem Glasses 28(6):215
6. Tuller HL, Button DP, Uhlmann DR (1980) J Non-Cryst Solids 40:93
7. Martin SW (1991) J Am Ceram Soc 74:1767
8. Elliot SR (1984) Physics of amorphous materials. Longman, New York
9. Martin SW, Angell CA (1986) J Non-Cryst Solids 83:185
10. Fujihara S, Sasaki C, Kimura T (2000) Key Eng Mater 181:109
11. Barbieri L, Corradi AB, Leonelli C, Siligardi C, Manfredini T, Pellacani GC (1997) Mater Res Bull 32(6):637
12. Pan A, Gosh A (2000) J Non-Cryst Solids 271:157
13. Villegas MA, Fernandez Navarro JM (2007) J Eur Ceramic Soc 27:2715
14. Tarte P (1962) Spectrochim Acta 18:467
15. Tarte P (1964) In: Prins IA (ed) Physics of non-crystalline solids. Elsevier, Amsterdam, p 549

16. Condrate RA (1972) In: Pye LD (ed) Introduction to glass science. Plenum Press, New York, p 101
17. Condrate RA (1986) J Non-Cryst Solids 84:26
18. Iordanova R, Dimitriev Y, Dimitrov V, Kassabov S, Klissurski D (1998) J Non-Cryst Solids 231:227
19. Iordanova R, Dimitriev Y, Kassabov S, Klissurski D (1996) J Non-Cryst Solids 204:141
20. Dimitrov V, Dimitriev Y, Montenero A (1994) J Non-Cryst Solids 180:51
21. Hutchinson JA, Allik TH (1992) Appl Phys Lett 60(12):1424
22. Salem SM, Shaltout I (2010) J Mater Sci 45:1837. Doi:10.1007/s10853-009-4167-3
23. Petru P, Lidia P, Rada S, Bosca M, Culea E (2008) J Vib Spectrosc 48:281
24. Motke SG, Yawale SP, Yawale SS (2002) Bull Mater Sci 25(1): 75
25. Bale S, Rahman S (2008) J Opt Mater 31:333
26. Baia L, Iliescu T, Simon S, Kiefer W (2001) J Mol Struct 259:9
27. Rusu D, Ardelean I (2008) J Mater Res Bull 43:1724
28. Pernice P, Aronne A, Catauro M, Marotta A (1997) J Non-Cryst Solids 210:23
29. Blaszczak K, Adamczyk A (2001) J Mol Struct 596:61
30. Marasinghe GK, Karabulut M, Ray CS, Day DE, Booth CH, Allen PG, Shuh DK (1998) Ceram Trans 87:261
31. Baiocchi E, Montenero A, Bettinelli M (1981) J Non-Cryst Solids 46:203
32. Nery SMD, Pontuschka WM, Isotani S, Rouse CG (1994) Phys Rev 49:3760
33. Austin IG, Mott NF (1969) Adv Phys 18:41
34. Qiu HH, Mori H, Sakata H, Hirayama T (1995) J Ceram Soc Jpn 103:32
35. Friedman L, Holstein T (1963) Ann Phys (NY) 21:494
36. Dhawan VK, Mansingh A, Sayer M (1982) J Non-Cryst Solids 51:87
37. Salem SM (2009) J Mater Sci 44:5760. doi:10.1007/s10853-009-3807-y
38. Nkum RK, Punnet A, Datars WR (1992) Physica C 202:371
39. Bogomolov VN, Kudinev EK, Firsov YuA (1968) Sov Phys Solid State 9:2502 Fiz Tverd Tela 9 (1967) 3175
40. Mott NF (1968) J Non-Cryst Solids 1:1
41. Mott NF, Davis EA (1979) Electronic processes in non-crystalline materials, 2nd edn. Clarendon Press, Oxford
42. Murali Krishna G, Srinivasa Reddy M, Veeraiah N (2007) J Solid State Chem 180:2747
43. Srinivasa Rao L, Srinivasa Reddy M, Krishna Rao D, Veeraiah N. J Solid State Sci. doi:10.1016/j.solidstatesciences.2008.06.022
44. Venkateswara Rao P, Satyanarayana T, Srinivasa Reddy M, Gandhi Y, Veeraiah N (2008) Physica B 403:3751
45. Ghosh A (1993) Phys Rev B 47:23
46. Prashant Kumar M, Sankarappa T, Kumar S (2008) J Alloys Compd 464:393
47. Shaaban MH, Ali AA, El-Nimr LK (2006) Mater Chem Phys 96:423
48. Sankarappa T, Prashant Kumar M, Devidas GB, Nagaraja N, Ramakrishnareddy R (2008) J Mol Struct 889:308
49. Mogus-Milankovic A, Licina V, Reis ST, Day DE (2007) J Non-Cryst Solids 353:2659
50. Raistrick LD, Macdonald JR, Franceschetti DR (1987) In: Macdonald JR (ed) Impedance spectroscopy. Wiley, New York (Chap. 2)
51. Cutroni M, Mandanici A, Piccolo A, Fanggao C, Saunders GA, Mustarelli P (1996) Soild State Ionics 90:167
52. Owen A (1963) Prog Ceram Soc 77:256
53. Elliott SR (1987) Adv Phys 36:135
54. Jain H, Mundy JN (1987) J Non-Cryst Solids 91:315
55. Elliott SR (1990) Physics of amorphous materials, 2nd edn. Longman, London
56. Shimakawa K (1982) Philos Mag B 46:123 (see also p 48, 77)
57. Mogus-Milankovic A, Santic A, Licina V, Day DE (2005) J Non-Cryst Solids 351:3235
58. Nageswara Rao P, Raghavaiah BV, Krishna Rao D, Veeraiah N (2005) J Mater Chem Phys 91:381